ЖЭТФ, 2004, том 126, вып. 4 (10), стр. 898–906

CARS STUDY OF DEUTERIUM CLUSTERS STABILIZED IN SOLID HELIUM

E. B. Gordon *

Institute of Problems of Chemical Physics, Russian Academy of Sciences
142432, Chernogolovka, Moscow region, Russia

T. Kumada, M. Ishiguro, Ya. Aratono

Advanced Science Research Center, Japan Atomic Energy Research Institute
319-1195, Tokai, Ibaraki, Japan

Submitted 27 April 2004

Solid deuterium clusters for the first time isolated in a matrix of solid Helium have been investigated at $T = 1.3$ K and $P = 3$ MPa by coherent anti-Stokes Raman spectroscopy (CARS) technique. The vibronic $Q_1(J = 0)$ and $Q_1(J = 1)$ line intensity, shape, and positions have been studied as functions of ortho- and para-content in the solid, as well as of the cluster size. The strong effect of Raman scattering cross section sensitivity to the molecular environment nuclear spin state has been found in CARS: the ratio of probabilities for the scattering by para ($J = 1$)- and ortho ($J = 0$)-deuterium being equal to 1 in a gas is as high as 10000 in nearly pure ortho-deuterium, whereas it is about 50 in spontaneous Raman scattering. This effect has been shown to occur starting from the cluster size corresponding to the phonon band onset.

PACS: 33.20.Fb, 33.70.Jg, 67.80.Mg

1. INTRODUCTION

The most inert matrix ever applied in the matrix isolation spectroscopy is para-hydrogen [1], only helium should be more inert than hydrogen in the symmetric $J = 0$ state (J is the rotational number). Because helium cannot be solid at ambient pressure, the conventional technique of matrix-isolation spectroscopy is inapplicable. Instead, the spectroscopic studies of molecules and clusters surrounded by helium were performed by the very interesting technique of their capture into cold liquid helium droplets. Although the molecule densities in the droplet experiments do not exceed those in the gas phase, the result of a photo-induced process could be detected with very high sensitivity by the depletion technique — the energy of visible and even infrared light photons released in a droplet induces evaporation of several thousand helium atoms, which is readily detectable if the droplet is sufficiently small. Although the finite size of a droplet, of course, causes some small distortion in the spectra observed, the approach allows obtaining very interesting information, mainly on quantum helium liquid interaction with microinclusions [2].

Meanwhile, the argument underlying the principal suggestions in [2], in particular, the effect of ^{4}He superfluidity on rotation of molecules and clusters embedded in liquid helium has been restricted by experimental impossibility to vary the matrix temperature and pressure in the framework of the droplet technique. The simplest solution could be the experiments at high pressure in a helium crystal doped by species under study, but just that has been widely accepted as impossible.

Nevertheless, the method of an impurity embedding into solid helium has been recently created [3, 4]. Among its first applications was the problem of matrix isolation spectroscopy of hydrogen; being the best material for isolation, hydrogen itself could not so far have been placed in a matrix more inert than it represents. Because of the high mobility of hydrogen molecules in solid helium [5], only molecular clusters can be stabilized in a helium crystal.

There is a very pronounced effect in the low-temperature vibrational $v = 0 \to v = 1$ Raman spectra of

*E-mail: gordon@binep.ac.ru

condensed molecular hydrogen, especially expressed for deuterium [6]: the ratio of the Raman scattering cross sections corresponding to the $Q_1(J=1)$ and $Q_1(J=0)$ transitions, which is equal to 1 in the gas phase, has been found to be strongly dependent on the concentration of molecules in the $J=1$ state in condensed phases; this ratio varies from 5 for nearly pure para ($J=1$)-deuterium (p = D_2) to 50 for nearly pure ortho deuterium (o = D_2) ($J=0$). This unexpectedly strong cooperative effect has been reliably explained for solid hydrogen and deuterium in [6] as caused by the delocalization of the $v=1$ impurity states in a crystal. However, at least two questions remain unanswered here: first, how this effect manifests itself in stimulated Raman scattering (RS) (while in spontaneous Raman scattering the transition probability is proportional to the square of the polarizability, the probability of coherent anti-Stokes Raman Scattering (CARS) is proportional to the square of the third-order susceptibility), and second, starting from what size of the microcrystal the ratio of the cross sections becomes large.

Although the size effect in Raman scattering by solid hydrogen should obviously exist and should be strong, nobody has discussed it, to our knowledge, possibly due to experimental impossibility to isolate small hydrogen clusters in a sufficiently inert matrix. Because the same effect has also been observed for liquid hydrogen and deuterium [7], it should not be too sensitive to crystal structure faults. Two cluster sizes may therefore be critical for the effect: first, that when the phonon band appears (it corresponds to about 10 layers of molecules in a crystallite and to the number of molecules in it about $N \approx 10^3$), and second, that when the crystallite size becomes comparable with the scattered light wavelength, i.e., when $N \approx 10^9$ (an ideal infinite crystal was considered in the calculations in [6]).

2. TECHNIQUES

Unlike in the case of heavier rare gases commonly used for matrix isolation, the introduction of impurities into solid helium represents a very sophisticated problem. Both liquid and solid helium are self-purified species because the solubility of any other substances is negligibly small in them. Epitaxial growth of a doped crystal from the gas phase is also impossible because helium is the only substance possessing no triple point and even no coexistence of gas and solid phases in equilibrium. Moreover, due to high plasticity of solid helium, a noticeable pressure gradient does not exist in it and the position of the liquid–solid interface in helium is governed only by the temperature profile, and hence the growth of a crystal from a liquid layer, which should be accompanied by the interface motion, is impossible. Only by using laser ablation from a target placed inside solid helium have the metallic clusters been stabilized trapped in solid helium in the very vicinity of a target [8, 9].

The technique that we use allows creating large doped helium crystals with impurities uniformly distributed in a bulk. The permanent growth of the crystal from its upper edge has been carried out under continuously moving the crystal body down at the account of helium exhaust from the crystal bottom; because of small friction of helium solid on a cell wall, even a very small pressure gradient is already sufficient for that motion. As a result, helium gas enters the cell from the gas supply system to restore the former crystal surface position by condensation. Thus, although both the position and shape of the crystal are visually unchanged with time, its contents permanently moves down with the velocity determined by the helium mass outflow.

As shown in Fig. 1, the experimental setup consists of an optical cell submerged into a liquid helium bath of the optical helium cryostat and a stainless steel gas-handling system. The body of the optical cell is a cylindrical sapphire tube (20 mm o.d., 17 mm i.d., and 80 mm length) put between indium-sealed brass flanges connected with the gas source at the top and with the outlet tube at the bottom. Sapphire has been chosen as simultaneously possessing the necessary strength for high-pressure operation, the optical transparency, and a reasonable thermal conductivity at low temperature. The gas source represents two coaxial thin-wall stainless tubes of 10 and 4 mm o.d., the inner one had an orifice 0.25 mm in diameter at its bottom to form the gas jet entering the optical cell. For thermal insulation, the space between the tubes has been pumped out and the lower end of the tubes was covered with teflon cap with an orifice in its center to allow the jet passage. The heater has been wired and glued to the surface of the inner tube along all its length inserted into the cryostat to keep the temperature in the tube well above the dew point temperature of dopant D_2; the temperature near the orifice was measured by a Cu-constantan thermocouple. Several layers of alumina mesh have been interposed to the bottom of the cell to provide uniformity of the outflow and to create a pressure gradient between solid helium in the optical cell and liquid helium in the outlet tube. To stabilize the position of the helium crystal upper interface, it was found useful to insert a constantan heater inside the outlet tube (the heating prevents the solidification of helium in the tube

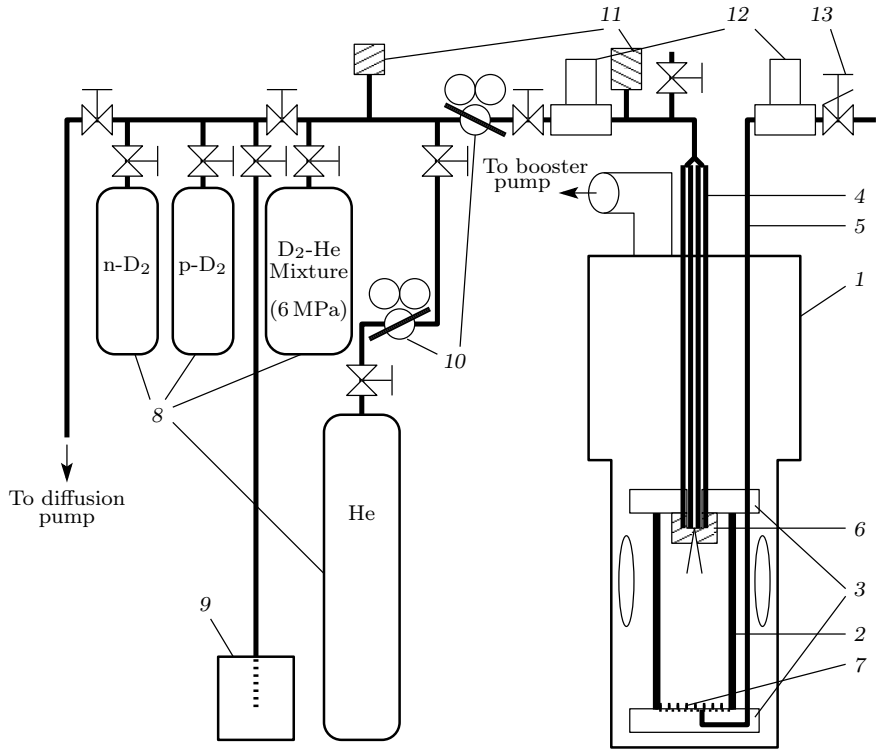

Fig. 1. Diagram of the optical cell, the He cryostat, and the stainless gas-handling system: *1* — cryostat, *2* — sapphire cell, *3* — brass flanges, *4* — double-walled inlet tube (a constantan heater and a thermocouple are glued to the inner tube), *5* — outlet tube (a constantan heater is inside), *6* — teflon cap, *7* — alumina mesh, *8* — gas cylinders, *9* — para–ortho converter, *10* — pressure regulators, *11* — pressure gauges, *12* — mass flow meters, *13* — needle valve

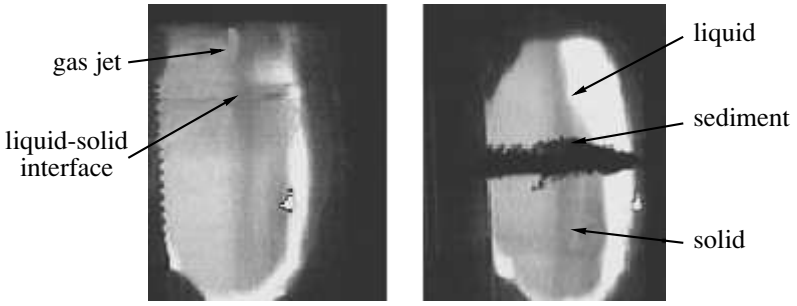

Fig. 2. Photos of a He crystal doped by 700 ppm of nitrogen: *a* — the procedure of sample preparation, $\Phi = 200$ sccm, $P = 3.15$ MPa, $T = 1.5$ K, the temperature of the orifice is around 250 K; *b* — crystal frontal melting by pressure decreasing to 2.6 MPa

violating stability of the outflow). The cell as a whole can be moved up and down by Wilson sealing at the cap of the cryostat, allowing study of the whole height of the grown sample.

Deuterium with enhanced abundance of o-D_2 was prepared by mixing normal deuterium (n-D_2) with o-D_2 produced in a cryocooler (Nagase & Co. Ltd. Model UV204SC) filled up by ferric oxide (FeO(OH)) catalyst at a temperature close to the D_2 triple point. Deuterium was then premixed with helium in the ratio $1 : 500 \sim 1000$ in a stainless steel cylinder at the pressure 6.0 MPa.

The procedure of sample preparation was as follows. During the pouring of the optical cryostat with liquid helium, the pure helium gas from the outer high-pressure cylinder was allowed to condensate in the cell

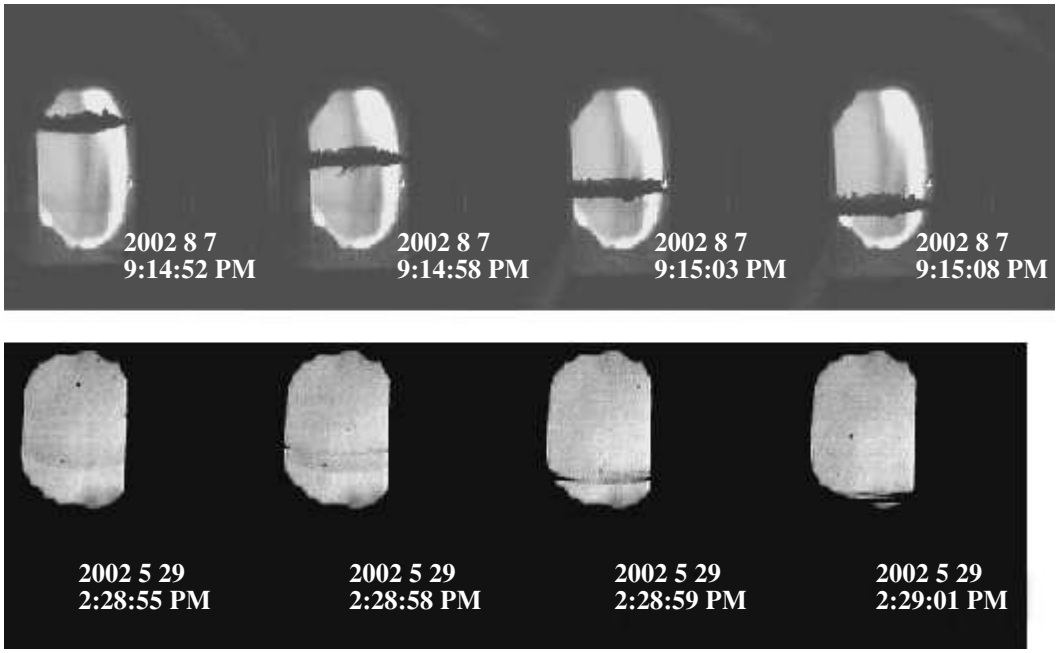

Fig. 3. Motion of the liquid–solid interface under diminishing helium pressure in real time for solid He doped by N_2 (upper) and by D_2 (lower), the window diameter is 3 cm

at the pressure about 1 MPa up to the filling of the entire cell by liquid helium and subsequent inflow termination; the cylinder was kept connected with the cell after that. Then the main helium bath of the cryostat was cooled by pumping with the booster (Shinko SMB-C60) and rotary (Alcatel T2063SD) pumps down to 1.2 K. The pressure of pure helium in the gas supply system was then increased to 2.8 MPa, the crystal was seen to grow in a few minutes after the pressures equalization (it was sometimes noticeable that a solid–solid transition occurred at the beginning, the moving up interface was clearly seen; that proceeded at a rather small pressure when, as follows from the phase diagram [10], the *bcc* phase of solid helium is formed previously and is then converted to the *hcp* phase under further cooling). After that, the needle valve at the end of the outlet tube was opened to start helium gas exhaust from the bottom of the optical cell, the outflow usually kept at 200–400 sccm (this corresponds to $(0.9–1.8)\cdot 10^{20}$ atoms per second). In steady conditions, the arising inflow was equal to the outflow; however, periodical jumps of the flows occurred, especially when the pressure in the cell was high enough. We believe that this happened when the pressure in the cell was more than 2.8 MPa (because of the impedance caused by the orifice, we cannot accurately determine that pressure in flow conditions) and the film of liquid helium covering the crystal surface was not consequently superfluid anymore (both normal liquid and solid helium have rather low thermal diffusivity [10]). Indeed, the liquid–solid interface was concave in the case showing that the main impedance for condensation heat removal is inside the cell. By decreasing the pressure, one could achieve the conditions when the interface became flat (the main impedance is the heat transfer through a sapphire wall) and stable. The photo in Fig. 2 demonstrates such a pattern. For growing a doped crystal, the flow of pure helium from the cylinder was replaced by that of a He-impurity mixture preliminarily prepared in the storage vessel. The typical rate of the D_2-doped helium crystal growth was 1 mm per minute. The pumping rate was high enough to keep the temperature of the bath less than 1.7 K during the sample preparation procedure when the heat release due to both the inlet heating and the gas mixture condensation was about 3 W. In all cases, the doped crystals were nicely transparent. After the sample preparation, the inflow of the He-impurity mixture was again replaced by the flow of pure helium for several minutes and then, keeping the pure helium supply system connected with the cell, the outflow was terminated and the inlet heater switched off. The sample thus prepared could be investigated for a long time without any noticeable changes.

The slow decrease of the pressure inside the cell

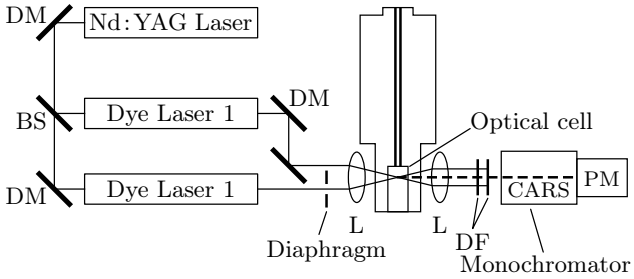

Fig. 4. Scheme of CARS detection: DM — dichroic mirror, BS — beam splitter, DF — dichroic filter, L — lense, PM — photomultiplier

by introducing a small outflow without any inflow led to frontal melting of the sample starting from its upper edge, as demonstrated in Fig. 3. The impurity from melted part of the crystal was then concentrated at the liquid–solid interface, forming a semitransparent sediment if the impurity content in the gas mixture was large. The interface and sediment motion could be ceased at a given position by stopping the outflow and opening the inflow to solidify the whole sample again. By vertical shift of the cell as a whole, the place with the enhanced impurity density could be placed into the observation zone.

The vibronic spectrum of coherent anti-Stokes Raman scattering of deuterium at our temperatures (around 1.5 K) consists of $Q_1(1)$ and $Q_1(0)$ transitions, the first of which belongs to p-D_2 and the second to o-D_2. The scheme of CARS measurements is presented in Fig. 4. Two light beams with the wavelengths 566 (green) and about 670–675 nm (red) from the tunable pulsed dye lasers (Lambdaphysik Scanmate and Lumonics Hyperdye-300) pumped by the second harmonic of a pulsed Nd:YAG laser with the 5 ns pulse duration and 10 Hz repetition rate (Continuum Powerlite 7000) were focused in one spot, usually near the axis of the optical cell. The CARS signal generated at the focal point was detected by a photomultiplier (Hamamatsu R-4220). Laser light and parasite luminescence were attenuated by dichroic filters and a monochromator (Nikon P-250) tuned to the wavelength of CARS emission. After integration by Boxcar (Stanford SR250), the CARS signal was digitized by an AD converter (Interface PCI3133) and was then accumulated in a personal computer. Using this technique, we could detect the $Q_1(1)$ and $Q_1(0)$ lines of gaseous deuterium even at the pressure 10^{-4} MPa with the frequency resolution about 0.5 cm^{-1}. As is known, the intensity of CARS signal I_{CARS} is

$$I_{CARS} \propto I_g^2 I_r n^2, \qquad (1)$$

where I_g and I_r are the respective intensities of green and red laser light and n is the density of deuterium molecules at the focal point.

3. EXPERIMENTAL RESULTS

The presence of solid helium in the cell resulted in the appearance of a rather intensive nonresonant blue signal, whose intensity was approximately proportional to I_g^2 and to I_r and the wavelength was equal to $2\omega_g - \omega_r$. The signal shown in Fig. 5 corresponds to nonresonant 4-wave scattering by helium. The probability of such a process is known to be proportional to the square of the nonresonant third-order susceptibility, which is 10 times less for helium than for deuterium and is equal to $4 \cdot 10^{-39}$ $cm^6/erg \cdot molecule$ [11]. The presence of an impurity in the helium crystal grown by condensation of the gas mixture containing rather small (less than 1000 ppm) amount of deuterium did not cause any significant change of this spectrum in either shape or intensity.

But if a part of the sample has been temporarily melted, the intensive narrow resonant deuterium signal is observed under focusing the laser beams to the former border between melted and nonmelted solid helium. The signal is stable in time (see Fig. 6).

Under the condensation of the gas mixture with large deuterium content, the resonant signal at a wavelength close to the deuterium line position exists from the very beginning (without preliminary melting) at the background of the nonresonant CARS signal. Its

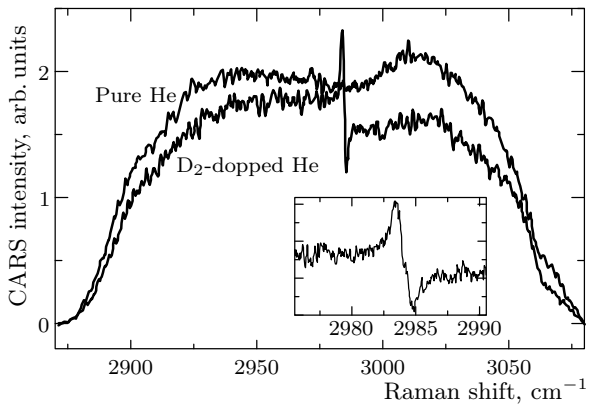

Fig. 5. CARS signal from pure He solid and from that doped by n-D_2 (2000 ppm). Apparent nonresonant signal shape is determined by the monochromator spectral width. The shape of D_2 line is shown in inset

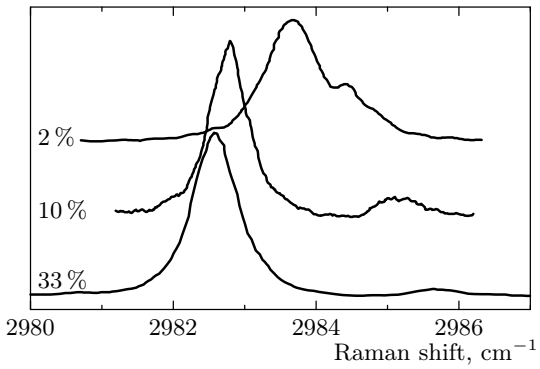

Fig. 6. CARS signal from D_2-doped solid He with the doped D_2 molecules (with different content of p-D_2 — 2, 10, and 33 %) concentrated by crystal temporal melting. The large left and small right peaks correspond to $Q_1(1)$ and $Q_1(0)$ transitions of D_2, respectively

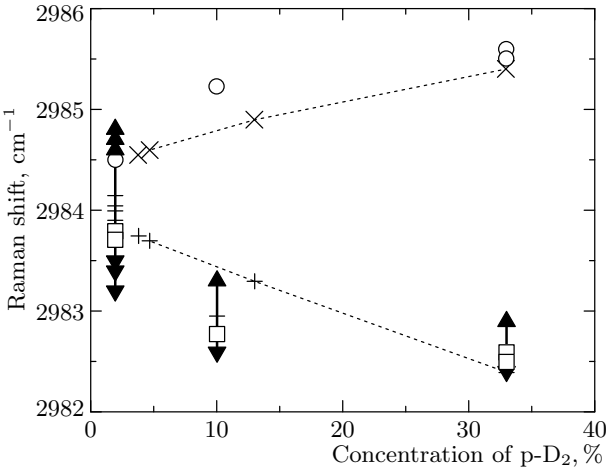

Fig. 7. D_2 Raman line positions vs ortho–para content in a mixture: distorted line for D_2 molecules trapped in solid He (▼ — negative peak, ▲ — positive peak), ◯, □ — o- and p-D_2 molecule lines in remelted solid He, ×, + — the same for solid D_2 from Ref. [16]

shape shown in Fig. 5 is typical of the resonance CARS signal superimposed on the intensive nonresonant background [12, 13]; the interference of these scatterings forms a so-called modulation dip distorting the line and «eating away» the background. The depth of the modulation dip shows that a significant part of nonresonant scattering originates from the focal point of laser beams, i.e., is caused by solid helium; the rest may proceed from the sapphire tube, optical windows, etc. It is worth mentioning that the CARS signal intensity was found to be independent of the focus point moving up and down or along the cell radius, thereby proving the uniformity of the stabilized cluster distribution in solid helium.

The impurity concentrating near the bottom of the «melted» zone during the crystal temporal melting evidences a large size of free inclusions formed by this procedure in condensed helium. Indeed, the height h of the region of the impurity cluster precipitation by gravity in liquid helium can be evaluated from the Boltzmann distribution

$$\frac{Nmgh}{kT}\,\frac{\rho_{D_2}-\rho_{He}}{\rho_{He}} \approx 1, \qquad (2)$$

where m is the deuterium mass, N is the number of molecules in a cluster, and ρ_{D_2} and ρ_{He} are the respective densities of solid deuterium and liquid helium. The height of the region with large cluster concentration estimated by the existence of an intensive CARS resonant signal is about 0.3 mm. This estimate gives $N = 10^8$, which corresponds to the cluster size 100 nm. The results of X-ray analysis of clusters formed by helium–deuterium jet injection directly to superfluid helium gave the size 3–6 nm [14]. But this estimate, made from the diffraction peak shape, represents a lower bound of the size because the width of the diffraction peak is sensitive not to the crystallite size but to the length of the crystalline structure regularity. Most probably, temporal melting of solid helium causes mutual gluing of small clusters, possessing rather regular structure into large particles.

The above observations allow accepting the following scenario.

The condensation of mixtures containing relatively small amount of deuterium (less than 1000 ppm) leads to the formation of rather small deuterium clusters distributed in bulk solid helium. As the content of the impurity in the gas mixture rises, the probability of molecule coalescence in a cooled gas jet just before its entering liquid helium and especially in liquid helium (during the particle motion to the solid–liquid interface) significantly increases and the clusters stabilized in solid helium become larger.

Finally, under helium crystal temporal melting, the clusters merge together in large objects precipitated by gravity. The cluster coalescence occurs in spite of the pressure being only about 1 bar less than that at the helium melting point; meanwhile the effective centripetal pressure caused by the Van der Waals interaction of the second layer of surrounding helium atoms with the deuterium core, being several bars, is therefore sufficient for keeping this layer solid even in a liquid [15].

It is reasonable to begin the analysis of CARS spectra of deuterium stabilized in solid helium from this

The ratios of probabilities of the $Q_1(1)$ and $Q_1(0)$ transitions for different contents of para-D_2 in a solid; for spontaneous RS, data were taken from [6], the CARS data are our results

	100 %	33 %	10 %	2 %
RS	5	10	30	50
CARS	?	150	1260	10000

sediment modeling a massive deuterium sample. In this case, the $Q_1(0)$ and $Q_1(1)$ line positions for different o-D_2 contents presented in Fig. 7 display a good fit to the literature data available for solid deuterium with o-D_2 content more than 20 % [6] and correctly reflect superlinear decrease of the $Q_1(0) - Q_1(1)$ splitting at small o-D_2 content observed recently [16] (the Fabri–Perrot resonator technique used in this work allows determining only splitting but not line positions).

It is immediately seen from Fig. 6 that even at the p-D_2 content as low as 2 %, the $Q_1(1)$ line is still much more intensive than the $Q_1(0)$ one (in the CARS spectrum of that mixture in a gas, we did not observe the $Q_1(1)$ line at all because it should be more than three orders of magnitude less intensive than the $Q_1(0)$ line). Taking into account that according to (1), the CARS signal intensity is proportional to the square of the scatterer concentration, we calculated the ratio of the probabilities of the $Q_1(1)$ and $Q_1(0)$ transitions in stimulated Raman scattering for deuterium crystallites with different ortho–para ratios. CARS line profiles both in a gas and in a solid were found to be nicely approximated by a Gaussian 0.62 cm^{-1} width, which probably represented the frequency resolution of our technique, and we simulated the line shape by this form in all cases. These probability ratios are compared in the Table with those known for common Raman scattering. One may easily notice that the crystal-field effect under consideration is much more pronounced in CARS: in deuterium containing 2 % of para modification, that ratio is as large as 10000, although it is only about 50 in Raman scattering [6].

For deuterium clusters isolated in solid helium (see Fig. 5), line distortion by a coherent interaction with the background does not allow precisely determining the position of the resonant CARS line. However, the peak of the ungarbled line should be positioned around half the distance between the maximum and the minimum of the distorted line [17], and as seen from Fig. 7, the signals for clusters with 10 % and 33 % p-D_2 content consist mainly of the $Q_1(1)$ lines. This means

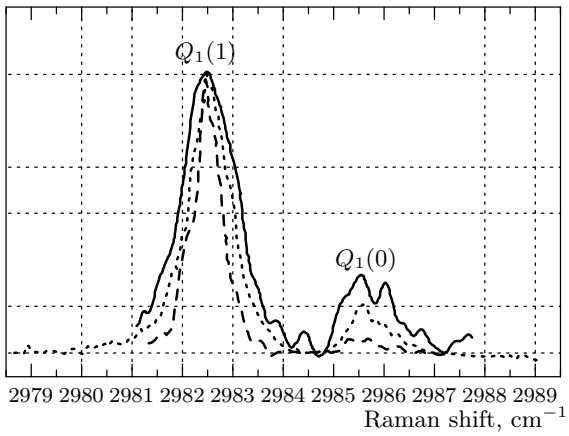

Fig. 8. $Q_1(1)$ and $Q_1(0)$ lines for He: n-D_2 crystal (T = 1.3 K, P = 3.15 MPa). Solid line — condensation of He gas containing 200 ppm of D_2. Dashed line — the same sample after fast annealing by decreasing the pressure to 2.6 MPa. Dotted line — solid obtained by condensation of He containing 1000 ppm of D_2

that for these clusters, presumably containing 10^3–10^4 molecules, the effect of the $Q_1(1)$ line predominance already exists: assuming the equal probabilities of $Q_1(0)$ and $Q_1(1)$ transitions, as is the case for the gas phase, the $Q_1(0)$ line intensity should be 10 and 100 times larger for n-D_2 and D_2 containing 10 % of para modification correspondingly. This effect seems to be anyway weaker than in a massive sample: in deuterium clusters containing 2 % of para modification, both the spectral width of the signal (much broader) and its position evidence that it actually consists of both $Q_1(1)$ and $Q_1(0)$ lines with comparable intensities, whereas in a sediment, the intensity of the $Q_1(1)$ line is still much higher than that of $Q_1(0)$ (see Fig. 6). This conclusion has been proved directly by comparing the line profiles before and after solid helium sample temporary melting; for a reliable line resolution, we then used n-D_2, where the $Q_1(0)$ and $Q_1(1)$ splitting is large enough. The results of such experiments presented in Fig. 8 clearly demonstrate that in smaller clusters, the lines are significantly more broadened and the ratio of their intensities is smaller.

4. DISCUSSION

In spite of the obvious presence of deuterium in solid helium bulk, no signal has been found for low deuterium content in a mixture when the smallest clusters are supposed to be stabilized. The low deuterium densities

should be not the only reason for the CARS observation failure. Indeed, we have reliably detected the CARS signal from gas deuterium at the density $3 \cdot 10^{17}$ cm^{-3}. In the experiments with solid helium, there was an extra noise connected with the instability of nonresonant scattering by solid helium, caused as usual by fluctuation of laser energies from pulse to pulse. But with the same line width, we should easily detect deuterium lines at the D_2 density about $3 \cdot 10^{18}$ cm^{-3} (100 ppm of deuterium in gas mixture). That means the deuterium lines from small clusters should be noticeably broadened, either by multiple faults of crystalline structure or due to large contribution from molecules located at a cluster surface where the matrix shift should be about half that in a bulk; both reasons should be valid only for small molecular clusters consisting of few layers. In principle, small clusters could be studied by using the delayed CARS [18]: because the helium third-order susceptibility should already be formed in femtoseconds and hydrogen CARS characteristic times are about a nanosecond even in a nonideal crystal, the nonresonant background may be removed there.

The modulation dip we have observed for larger deuterium clusters stabilized in solid helium can be used for measurement of the helium nonresonant third-order susceptibility $\gamma^{(3)}_{non}$ by the procedure proposed in [19] and applied there for the argon $\gamma^{(3)}_{non}$ determination from the analysis of the modulation dip shape of the nitrogen CARS signal. Although the $\gamma^{(3)}_{non}$ value of helium is of general interest [12], the accuracy of its literature value is far from being satisfactory. Owing to a small $\gamma^{(3)}_{non}$ value, it is difficult to measure it in a helium gas; this has been impossible unless by embedding small (less than λ) separated optically active impurities into condensed helium.

Surprisingly, although the $Q_1(0)$ and $Q_1(1)$ lines in condensed hydrogen and deuterium have been extensively studied by Raman scattering, the CARS technique has not been used for that. Our results for deuterium sediment in re-melted solid helium should therefore be considered the first study of a large effect of the surrounding nuclear spin modification on the $Q_1(0)$ and $Q_1(1)$ transition probability ratio in solid deuterium by the CARS technique. From a general standpoint, such an effect should be much stronger in CARS than in Raman scattering. Indeed, in the harmonic oscillator approximation valid for simple molecules, $\gamma^{(3)}_{res} \propto \alpha^2$, where α is the polarizability and $\gamma^{(3)}_{res}$ is the third-order susceptibility at a resonance [20], and there is a simple relation between the ratios of the $Q_1(1)$ and $Q_1(0)$ line intensities in spontaneous RS and in CARS,

$$\frac{I_{CARS}(1)}{I_{CARS}(0)} = \left(\frac{I_{RS}(1)}{I_{RS}(0)}\right)^2. \qquad (3)$$

The data in the Table show that this is nearly true. Nevertheless, one may notice that the effect is anyway stronger than it follows from (3): for example, in Raman scattering experiments [6] for deuterium crystals containing 2 % of para modification, the intensities of $Q_1(1)$ and $Q_1(0)$ lines are nearly the same, whereas in CARS, as is seen from Fig. 6, the $Q_1(0)$ line is significantly weaker. By the way, this effect may be used for determination of completeness of the para–ortho conversion in deuterium with a sensitivity better than 10^{-3} %.

The impossibility to detect the resonant CARS signal in small clusters does not allow us to fully trace size dependence of the effect — it already exists when the resonant deuterium peak appears in our experiments. That is the evidence that the effect of huge predominance of the CARS accompanied by $Q_1(1)$ transition develops together with phonon band formation in a deuterium cluster. But the transfer to a large probability ratio proceeds gradually: we have managed to observe the enhancement of the effect as the cluster size grows further (see Fig. 5), synchronously with the line narrowing.

5. CONCLUSION

The promises of the new technique of embedding impurities into solid helium have been demonstrated with the example of deuterium cluster stabilization in that matrix, more inert than hydrogen. It was experimentally shown that the impurity clusters are distributed homogeneously in the helium crystal; this opens the possibility to use laser irradiation to evaporate the separate molecules from the clusters preliminarily stabilized in solid helium, as has been done in [8, 9] for metallic atoms.

The extremely strong dependence of the third-order resonant susceptibility related to $Q_1(0)$ and $Q_1(1)$ transitions in solid deuterium on the ratio of ortho–para modifications has been found. Of course, this effect must exist in a massive deuterium crystal and also in hydrogen. It is significant that in spontaneous Raman scattering, the effect of the $J = 1$ transition dominance consists of a redistribution of the probabilities of scattering by ortho and para states, with the total cross section being independent of their content [6]. This should not be true for stimulated Raman scattering

where the probabilities are proportional to square of the species concentration.

The phenomenon of the $J = 1$ Raman scattering dominance has been found to occur just as the size of deuterium crystallite becomes sufficient for phonon band formation.

Nonresonant CARS from solid helium has been observed for the first time; in a crystal doped by small clusters of Raman-active molecules, the modulation dip of their CARS line made it possible to calculate the absolute value of the nonresonant third-order susceptibility for helium.

This work was supported in part by the Grant-in-Aid for Scientific Research of the Ministry of Education, Culture, Sports, Science, and Technology of Japan. E. G. appreciates the support from the JAERI Foreign Researcher Inviting Program and from the RFBR (grants №№ 00-15-97400, 01-03-32247). The authors are grateful to T. Momose for useful discussions.

REFERENCES

1. T. Oka, Ann. Rev. Phys. Chem. **44**, 299 (1993).
2. S. Grebenev, J. P. Toennies, and A. F. Vilesov, Science **279**, 2083 (1998).
3. E. B. Gordon, A. Usenko, and G. Frossati, J. Low Temp. Phys. **130** (112), 15 (2003).
4. E. B. Gordon, G. Frossati, A. Usenko et al., Physica B **329–333**, 404 (2003).
5. V. A. Mikheev, B. A. Maidanov, and N. P. Mikhin, Sov. J. Low Temp. Phys. **9**, 901 (1983).
6. J. Van Kronendonk, *Solid Hydrogen, Theory of the Properties of Solid* H_2, HD, *and* D_2, Plenum, New York (1983).
7. S. S. Bhatnagar, E. J. Allin, and H. L. Welsh, Can. J. Phys. **40**, 9 (1962).
8. S. I. Kanorsky and A. Weis, Adv. Atom., Molec. Opt. Phys. **38**, 87 (1997).
9. K. Ishikawa, A. Hatakeyama, K. Gosyono-o et al., Phys. Rev. B **56**, 780 (1997).
10. J. Wilkes, *Properties of Liquid and Solid Helium*, Oxford University Press (1959).
11. T. Lundeen, S.-Y. Hou, and J. W. Nibler, J. Chem. Phys. **79**, 6301 (1983).
12. J. W. Hahn, S. N. Park, E. S. Lee et al., Appl. Spectr. **47**, 710 (1993).
13. M. D. Levenson, IEEE J. Quant. Electron. **QE-10**, 110 (1974).
14. S. I. Kiselev, V. V. Khmelenko, D. M. Lee et al., Phys. Rev. B **65**, 024517 (2002).
15. E. B. Gordon and A. F. Shestakov, Low Temp. Phys. **26**, 1 (2000).
16. J. L. Fredman, J. H. Eggert, J. D. Kinder et al., J. Low Temp. Phys. **115**, 181 (1999).
17. N. Bloembergen, *Nonlinear Optics*, World Scientific, River Edge, NJ (1996).
18. M. Karavitis, R. Zadoyan, and V. A. Apkarian, J. Chem. Phys. **114**, 4131 (2001).
19. K. Akihama, T. Asai, and S. Yamazaki, Appl. Opt. **32**, 7434 (1993).
20. S. A. Akhmanov and N. I. Koroteev, *Methods of Nonlinear Optics in Spectroscopy of Light Scattering*, Nauka, Moscow (1981) (in Russian).